Electronic Supporting Information

A robust and stable phenolic resin-crosslinked graphene aerogel for efficient solar-driven steam-power co-generation

Chuchu Zhang,[a#] Jiapeng Song,[a#] Yanjun Li,[b] Jiaqi Chen,[a] Zhuoli Yang,[a] Yuanjin Wang,[a] Tao Liu,[a] Long Chen,[a] Zhenggang Rao,[a] and Linfeng Fei[a]**

a School of Physics and Materials Science, Jiangxi Provincial Key Laboratory of Photodetectors, Nanchang University, Nanchang, Jiangxi 330031, China

b School of Chemistry and Chemical Engineering, Jiangxi Science and Technology Normal University, Nanchang, Jiangxi 330038, China

* *Corresponding authors.*

E-mail address: feilinfeng@gmail.com (L. Fei); raozhenggang@ncu.edu.cn (Z. Rao).

[#] Chuchu Zhang and Jiapeng Song contribute equally to this work.

Table of contents

Supporting Figures

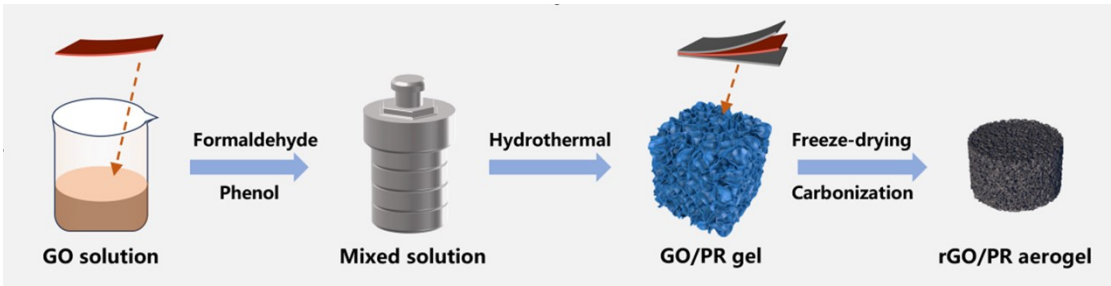

Figure S1 Schematic illustration for the synthesis process of the rGO/PR aerogel.

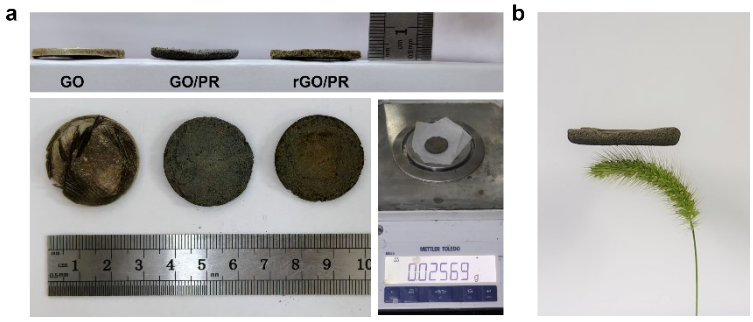

Figure S2 (a) Dimensions photographs of the GO, GO/PR, rGO/PR aerogels and weight photograph of a rGO/PR aerogel. (b) Physical image of a rGO/PR aerogel on a grass.

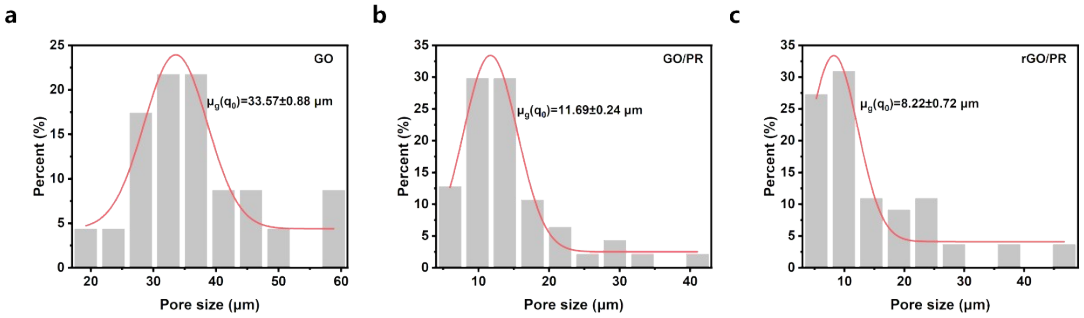

Figure S3 Frequency distribution of the pores' diameters for (a) GO, (b) GO/PR, and (c) rGO/PR aerogels (analyzed from SEM images).

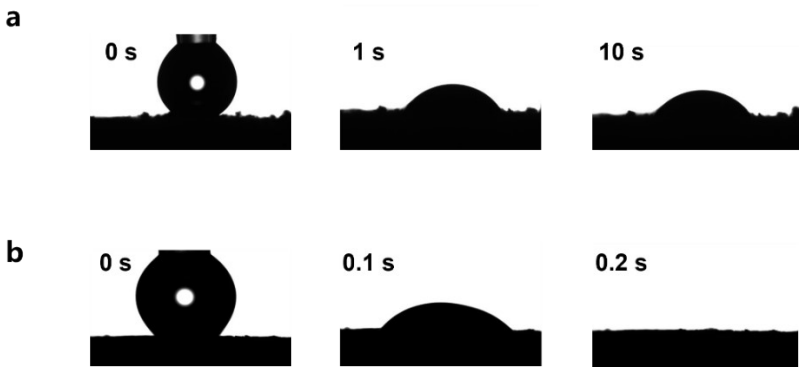

Figure S4 Water contact angles of (a) GO and (b) GO/PR aerogels v.s. time.

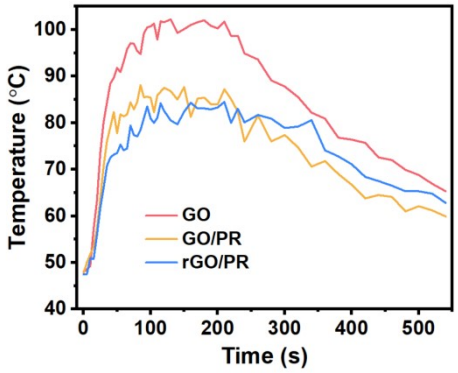

Figure S5 Surface temperature profiles of three aerogels placed on a heating plate at 150 ℃.

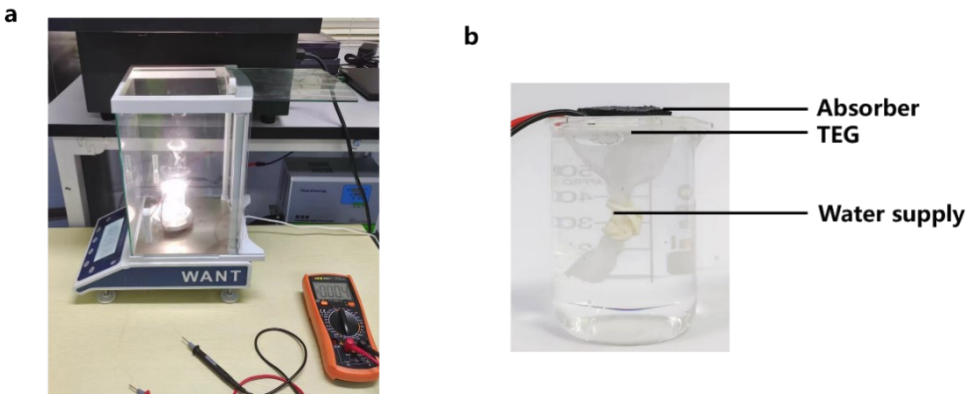

Figure S6 (a) Photograph of the co-generation system. (b) Enlarged view of the co-generation device.

Figure S7 Photographs of the GO aerogel before and after water absorption.

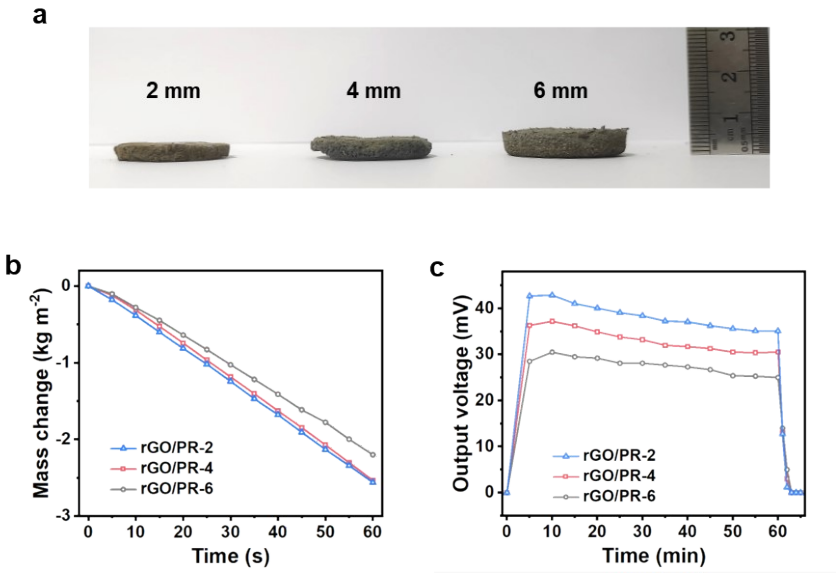

Figure S8 (a) Photograph of the aerogels with different thicknesses. (b) Water mass changes for the three samples with different thicknesses in a simulated sunlight exposure. (c) Output voltage for the three samples with different thicknesses.

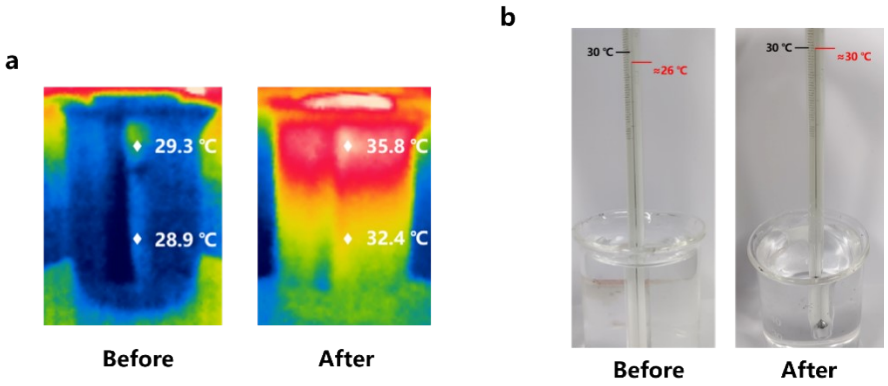

Figure S9 (a) Infrared images and (b) photographs of water temperature before and after three evaporation cycles.

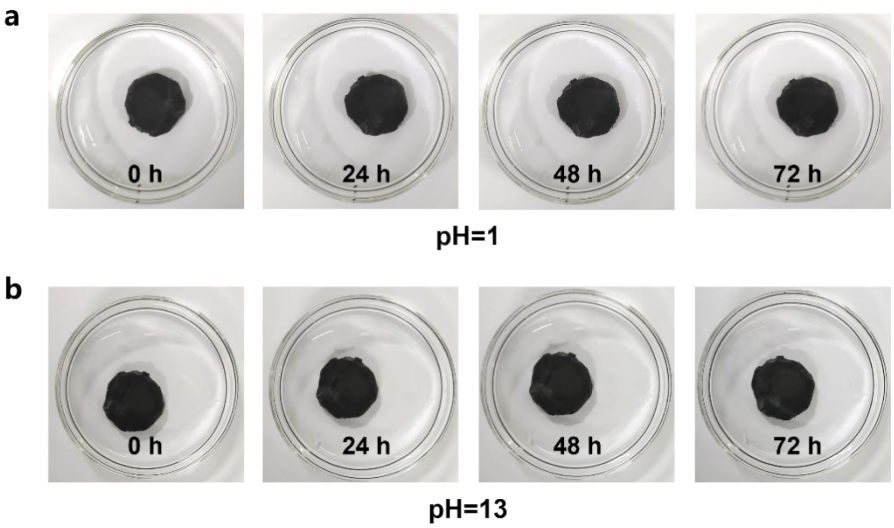

Figure S10 Photographs of the rGO/PR aerogel in solutions of (a) pH=1 and (b) pH=13 for 72h.

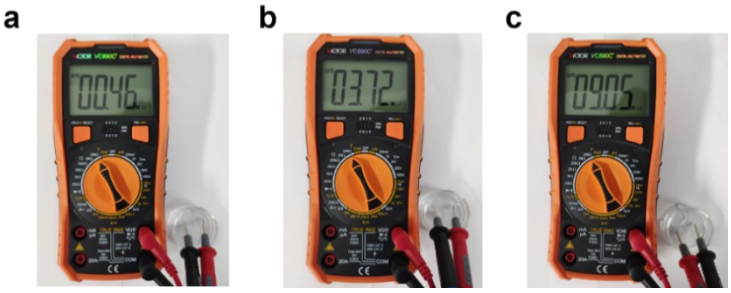

Figure S11 Resistances of (a) simulated seawater, (b) domestic water and (c) the condensate from the evaporation treatment.

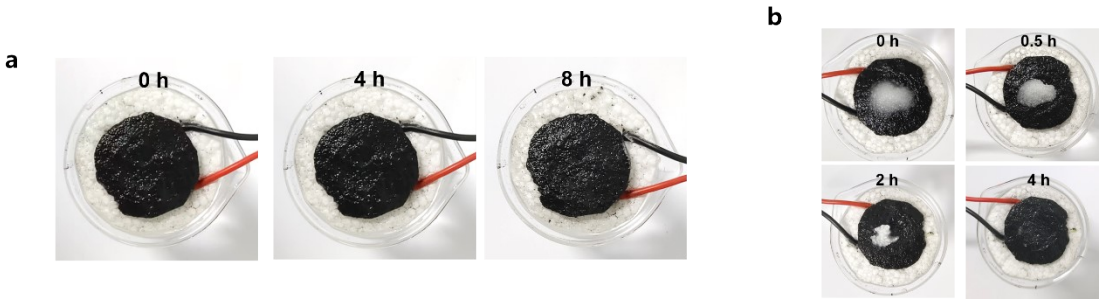

Figure S12 (a) Time-dependent salt buildup on the rGO/PR aerogel's surface. (b) Optical photo series of the rGO/PR aerogel loaded with 0.3 g NaCl powder floating on simulated seawater under one sun illumination for 4 h.

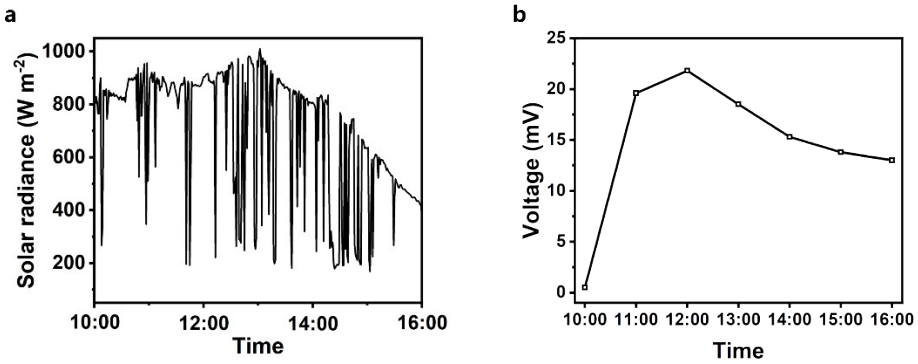

Figure S13 (a) Time-dependent solar radiance profile at Nanchang, Jiangxi, China on Aug. 2, 2024. (b) Time-dependent of voltage profile for the SSG device.

Supporting Notes

Note S1. Calculation of the pore diameters for the GO, GO/PR, and rGO/PR aerogels.

We have measured the diameters of the pores for the GO, GO/PR, and rGO/PR aerogels, and the results are as follows (**Tables S1-S3**).

Note S2. Calculation details for the conversion efficiency.

During photothermal evaporation of water, SSG conversion efficiency can be found through determining heat loss.[1] The energy consumption of solar evaporator mainly includes: (1) energy losses of reflectance and transmittance; (2) energy for water evaporation; (3) conduction heat loss from aerogels to the bulk water; (4) radiation loss of aerogels to the surrounding environment and (5) convective heat loss. Therefore, the theoretical solar steam conversion efficiency (η_{eva}) can be calculated by the following formula:[2]

$$\eta_{eva} = \eta_{abs} - \eta_{cond} - \eta_{rad} - \eta_{conv} \quad \textbf{Equation S1}$$

(1) Conduction heat loss η_{cond}

The conduction loss can be calculated as:

$$P_{cond}=Cm\Delta T/\mathrm{t} \quad \textbf{Equation S2}$$

Where C is the specific heat capacity of water (4200 J kg^{-1} K^{-1}), m is the mass of the water body, and ΔT is the temperature difference before and after water evaporation, t is time of water evaporation.

(2) Radiation heat loss η_{rad}

The radiation loss can be calculated by the Stefan-Boltzmann equation:

$$P_d=\varepsilon A\sigma(T_1^4-T_2^4) \quad \textbf{Equation S3}$$

Where ε is the emissivity of the surface of aerogels (i.e., 0.9534 for the rGO/PR aerogel), A represents the surface aera of aerogels (i.e., 5.307 cm^2 for the rGO/PR aerogel), σ is the Stefan-Boltzmann constant (5.67×10^{-8} W m^{-2} K^{-4}), T_1 and T_2 are the surface temperature of the aerogel at stable state and the environment temperature, respectively. Particularly, because the surface of aerogels is surrounded by water and its vapor, the temperature of the environment on top of the absorber is close to that of the aerogels. Therefore, a thermocouple was utilized to measure the temperature near the top of the absorber surface (the temperature of the rGO/PR aerogel is about 38 °C).

(3) Convection heat loss η_{conv} **Equation S4**

The convection loss can be calculated according to Newton's law of cooling:

$$P_{conv} = hA(T_1 - T_2)$$

Where h denotes convection heat transfer coefficient (5 W m^{-1} K^{-1}).

Based on the above equations, as shown in **Table S5** below, the photothermal conversion efficiencies of the GO/PR and rGO/PR aerogels are 89.34% and 92.21%, respectively.

Note S3. Variations of water state with the rGO/PR aerogel.

Aerogels can adsorb numerous water molecules due to their hydrophilicity, forming three distinct water states: bound water, intermediate water (IW), and free water (FW). Bound water strongly interacts with the hydrophilic groups of aerogels and does not participate in evaporation, thus its contribution can be neglected. FW exhibits no interaction with the aerogel's surface groups. IW represents a transitional state between bound water and free water (aerogels weakly interact with surrounding water molecules).[3] Consequently, in a water evaporation device, a higher proportion of intermediate water reduces the energy required to evaporate the same mass of water (corresponding to a lower evaporation enthalpy and an improved evaporation rate).[4]

In our study, the hydrophilic groups on the rGO/PR aerogel form strong electrostatic interactions and hydrogen bonds with water molecules, resulting in increased intermediate water molecules. We also used Raman spectroscopy to study the different water states around the aerogel. Specifically, the peaks at 3230 and 3360 cm^{-1} are indicative of FW molecules, while those at 3490 and 3610 cm^{-1} correspond to IW molecules. The calculated ratios of IW/FW for pure water and rGO/PR aerogel are 0.62 and 0.76, respectively; thereby, the aerogel lowers the enthalpy of evaporation and improves the conversion efficiency during evaporation.

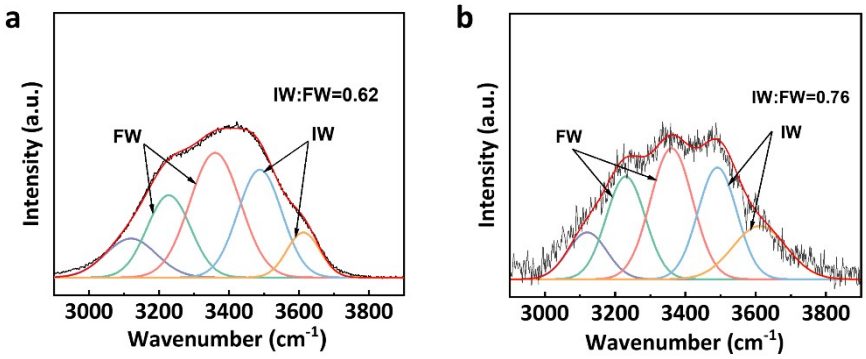

Figure S14 Raman spectra with fitting curves of FW and IW in (a) pure water and (b) rGO/PR aerogel.

Supporting Tables

Table S1. Frequency distributions for pore diameters of GO aerogel as shown in **Figure 1j**.

Diameter (μm)	**19.2**	**23.6**	**28**	**32.4**	**36.8**	**41.2**	**45.8**	**50**	**54.4**	**58.8**
Percent (%)	**4.35**	**4.35**	**17.39**	**21.74**	**21.74**	**8.7**	**8.7**	**4.35**	**0**	**8.7**

Table S2. Frequency distributions for pore diameters of GO/PR aerogel as shown in **Figure S2a**.

Diameter (μm)	**5.95**	**9.85**	**13.75**	**17.65**	**21.55**	**25.45**	**29.35**	**33.25**	**37.15**	**41.05**
Percent (%)	**12.77**	**29.79**	**29.79**	**10.64**	**6.38**	**2.13**	**4.26**	**2.13**	**0**	**2.13**

Table S3. Frequency distributions for pore diameters of rGO/PR aerogel as shown in **Figure S2b**.

Diameter (μm)	**5.3**	**9.9**	**14.5**	**19.1**	**23.7**	**28.3**	**32.9**	**37.5**	**42.1**	**46.7**
Percent (%)	**27.27**	**30.91**	**10.91**	**9.09**	**10.91**	**3.64**	**0**	**3.64**	**0**	**3.64**

Table S4. Comparison of the wettability of the rGO/PR aerogel with other reported materials by the time it takes to absorb a drop of water.

No. #	Materials	Infiltration time (s)
1	GO-1[5]	58
2	GPF[6]	~25
3	PP[7]	180
4	SBCA[8]	30
5	CMPA[9]	165
6	PPy@TA–Ti PTM[10]	260
7	SCBP[11]	25
8	This work	10

Table S5. Calculations of conduction, convection, radiation, and photothermal conversion efficiencies of the GO/PR and rGO/PR aerogels.

	GO/PR	rGO/PR
η_{abs}	95.17%	95.34%
η_{cond}	0.12%	0.12%
η_{rad}	0.009%	0.0078%
η_{conv}	5.7%	3%
η_{eva}	89.34%	92.21%

Table S6. Comparison of evaporation rates and power density for the rGO/PR aerogel and other reported materials.

No. #	Materials	ER (kg m^{-2} h^{-1})	PD (W m^{-2})
1	CC-BPHPLS [12]	0.804	0.115
2	CBAP [13]	1.900	0.015
3	PMD/MXene-WCM [14]	1.59	0.71
4	CP@PVA [15]	2.23	1.04
5	MCS1 [16]	2.67	0.42
6	PNPG/MoS_2 [17]	1.70	0.23
7	B700 [18]	1.21	~0.9
8	CPC [19]	1.38	~0.3
9	SAWH-TEPG [20]	0.75	0.685
10	Ag-Cu/SDB@PVA [21]	1.49	0.034
11	CuS-rGO [22]	2.29	1.32
12	GOM [23]	1.6	0.9
13	P-g-C_3N_4@rGO/DB [24]	1.98	0.01369
14	GFGP [25]	2.3	0.46
15	This work	2.64	0.987

ER stands for evaporation rate (kg m^{-2} h^{-1}) and PD stands for power density (W m^{-2}).

Table S7. Comparison of the magnitude of strain resistance of rGO/PR aerogels and other reported graphene-based materials.

No. #	Materials	Strain (%)
1	CPG-Ag[26]	50
2	PHEMA/SA-Ca^{2+}/rGO[27]	~40
3	PEI-GOs/PVA[28]	40
4	PArG[29]	30
5	GR/PPy-30[30]	~20
6	This work	70

References

[1] C. Onggowarsito, S. Mao, X. S. Zhang, A. Feng, H. Xu, Q. Fu, *Energy Environ. Sci.* **2024**, 17, 2088.

[2] Y. Wang, J. Hu, L. Yu, X. Wu, Y. Zhang, H. Xu, *Nano Res. Energy* **2023**, 2, e9120062.

[3] X. Zhou, Y. Guo, F. Zhao, W. Shi, G. Yu, *Adv. Mater.* **2020**, 32, e2007012.

[4] Y. Wang, Y. Li, Q. Huang, W. Qi, R. Zan, M. Gan, Z. Rao, L. Fei, *Desalination*, **2023**, 566, 116910.

[5] L. Chen, J. Wei, Q. Tian, Z. Han, L. Li, S. Meng, Q.-M. Hasi, *Langmuir* **2021**, 37, 10191.

[6] L. Bian, L. Jia, Y. Zhou, H. Gang, Z. Wang, Y. Zhou, S. Gu, X. Liu, W. Xu, Y. Zhuang, H. Yang, *Mater. Today Commun.* **2022**, 33, 104337.

[7] S. Sun, Y. Wang, B. Sun, F. Zhang, Q. Xu, H.-Y. Mi, H. Li, X. Tao, Z. Guo, C. Liu, C. Shen, *ACS Appl. Mater. Interfaces* **2021**, 13, 24945.

[8] D. Wei, X. Cao, M. Ma, Z. Zhao, J. Zhang, X. Dong, C. Wang, *Glob. Chall.* **2023**, 7, 2300046.

[9] Y. Wang, Y. Li, Q. Huang, W. Qi, R. Zan, M. Gan, Z. Rao, L. Fei, *Desalination* **2023**, 566, 116910.

[10] X. Zhao, Y. Lan, T. Wang, Y. Jiang, J. Pan, *J. Mater. Chem. A* **2022**, 10, 13895.

[11] J. Li, R. Lv, G. Li, W. Luo, J. Wang, M. Xia, P. Zhao, Y. Chen, S. Wu, Q. Chen, Y. Shen, M. Li, W. Xiao, W. Dong, J. Xiao, *Desalination* **2023**, 567, 116954.

[12] Y. Xu, Z. Guo, J. Wang, Z. Chen, J. Yin, Z. Zhang, J. Huang, J. Qian, X. Wang, *ACS Appl. Mater. Interfaces* **2021**, 13, 27129.

[13] Z. Li, X. Ma, D. Chen, X. Wan, X. Wang, Z. Fang, X. Peng, *Adv. Sci.* **2021**, 8, 2004552.

[14] J. Wu, T. Li, Q. Zhao, X. Wen, L. Liu, J. Duan, *Sustainable Mater.Technol.* **2024**, 40, e00950.

[15] X. Zhao, Z. He, W. Ou, P. Lin, Y. Chen, Y. Chen, *Sci. China Mater.* **2022**, 65, 2491.

[16] R. Niu, J. Ren, J. J. Koh, L. Chen, J. Gong, J. Qu, X. Xu, J. Azadmanjiri, J. Min, *Adv. Energy Mater.* **2023**, 13, 2302451.

[17] Z. Lin, T. Wu, Y.-F. Feng, J. Shi, B. Zhou, C. Zhu, Y. Wang, R. Liang, M. Mizuno, *ACS Appl. Mater. Interfaces* **2022**, 14, 1034.

[18] A. Ghaffar, M. Usman, M. U. Khan, M. Hassan, *J. Cleaner Prod.* **2024**, 446, 141374.

[19] H. Li, S. Wang, Z. Yan, X. Niu, X. Sun, W. Hong, *Appl. Therm. Eng.* **2022**, 208, 118279.

[20] T. Li, M. Wu, J. Xu, R. Du, T. Yan, P. Wang, Z. Bai, R. Wang, S. Wang, *Nat. Commun.* **2022**, 13, 6771.

[21] A. G. Saad, A. Gebreil, D. A. Kospa, S. A. El-Hakam, A. A. Ibrahim, *Desalination* **2022**, 535, 115824.

[22] L. Zeng, D. Deng, L. Zhu, Z. Zhang, X. Gu, H. Wang, Y. Jiang, *Nano Energy* **2024**, 125, 109531.

[23] A. Ghaffar, Q. Imran, M. Hassan, M. Usman, M. U. Khan, *J. Environ. Chem. Eng.* **2022**, 10, 108424.

[24] A. G. Saad, S. A. El-Hakam, A. I. Ahmed, A. A. Ibrahim, A. Gebreil, *J. Water Process Eng.* **2024**, 58, 104840.

[25] Q. Zhao, H. Wen, J. Wu, X. Wen, Z. Xu, J. Duan, *Desalination* **2024**, 570, 117064.

[26] L. Geng, X. Zhang, Y. Li, G. Feng, X. Yu, *Langmuir* **2024**, 40, 13412.

[27] X. Liu, K. Zhang, J. Wang, *Chem. Eng. J.* **2024**, 484, 149490.

[28] Z. Yang, Y. Liu, K. Xue, P. Fu, F. Du, Y. Zhang, *Mater. Today Commun.* **2023**, 35, 106195.

[29] P. Mu, L. Song, L. Geng, J. Li, *Sep. Purif. Technol.* **2021**, 271, 118869.

[30] S. Yan, H. Song, Y. Li, J. Yang, X. Jia, S. Wang, X. Yang, *Appl. Catal., B* **2022**, 301, 120820.